Nanoscale

Accepted Manuscript

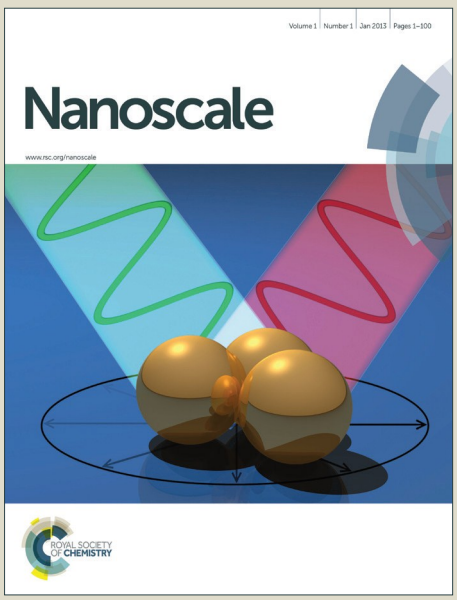

ROYAL SOCIETY OF CHEMISTRY

www.rsc.org/nanoscale

Journal Name

ARTICLE TYPE

Cite this: DOI: 10.1039/xxxxxxxxxx

Received Date
Accepted Date

DOI: 10.1039/xxxxxxxxxx

www.rsc.org/journalname

Charging C_{60} Islands with the AFM Tip †

Brice Hoff,[a] Claude R. Henry,[a] and Clemens Barth*[a]

We show that electrons can be transferred on demand from the AFM tip into single bulk-like C_{60} islands, which are supported on the insulating NaCl(001) surface. We exemplify this by controlled charge-manipulation experiments conducted in ultrahigh vacuum by noncontact AFM (nc-AFM), electrostatic force microscopy (EFM) and Kelvin probe force microscopy (KPFM). KPFM shows a homogeneous contrast at the islands, which is a signature for an equal distribution of the electrons in the T_{1u} band. The charge dissipates during half a day due to an interaction of the charged C_{60} islands with defects in the near surface region of NaCl. Our results open the perspective in photovoltaic to study charge attachment, stability and charge exchange with the environment of a C_{60} bulk-like system.

1 Introduction

Since their experimental discovery in 1985[1], buckminsterfullerenes (C_{60}) have been subject for many investigations[2] like in superconductivity[3], biochemistry[4] and in particular in the domain of photo-voltaic, where fullerenes and derivatives are used in two-dimensional organic thin films[5]. Based on weak van der Waals forces, C_{60} molecules crystallize at room temperature into a solid with a fcc lattice[6,7], which has fascinated research ever since as exemplified by the large amount of scanning tunneling microscopy (STM) work on thin C_{60} films[8]. STM gives great insights into phenomena of self-assembly[9,10], and even the orientation of single C_{60} molecules can be studied with high precision[11]. The molecules have been also imaged by noncontact atomic force microscopy on in particular insulating surfaces[12–17]. As shown by the revolutionary nc-AFM work of the Meyer group[18], the inner atomic structure of a C_{60} molecule can be resolved at low temperatures[19], with an unmatched precision in comparison to STM[20].

A fascinating property of the single C_{60} molecule is that due to its large electron affinity of $EA_{mol} = 2.6$ eV and low activation energy for electron attachment the molecule is a good electron acceptor[21–23]: a free C_{60} molecule can accept several electrons with the single anion C_{60}^- being relatively stable[24,25]. With respect to bulk C_{60}, calculations exhibit a semi-conducting character of the solid due to the H_u band being completely filled with electrons and the empty T_{1u} band, both separated by a band gap of about $E_{gap} \sim 2.6$ eV[26]. The electron affinity increases when C_{60} is in bulk form reaching a value of $EA_{bulk} \sim 3.6$ eV[27,28]. When in particular thin films of C_{60} are grown on metal surfaces an intrinsic charge transfer between the metal and the film takes place[29] as exemplified by the work of Modesti and collaborators[30]: a growth of C_{60} islands on Au(110)c2×2 leads to a charge transfer of 2 electrons/molecule at the interface. Even more, in the presence of a mono-layer (ML) of potassium on the same gold surface the amount of transferred charge raises to 3 electrons/molecule with the largest charge transfer of 6 electrons/molecule when the film is supported on a very thick potassium film. Such experiments could be enriched by the observation that alkali atoms can be intercalated in the C_{60} solid[31,32], as demonstrated by STM experiments in the Crommie group on K/C_{60} films supported on Au(111)[33,34]: electrons are transferred from potassium to the C_{60} molecules and when increasing the amount of potassium from K_3C_{60} to K_4C_{60} the C_{60} film changes its electronic configuration from insulating to metallic.

In the past, the direct capture of electrons by single C_{60} molecules was realized by crossing an electron beam with a molecular beam of C_{60}, which yielded important information about, e.g., the lifetime of single C_{60} anions[25]. The *curious* ques-

[a] CNRS, Aix-Marseille University, CINaM UMR 7325, Campus de Luminy, Case 913, 13288 Marseille Cedex 09, France. Fax: +33 (0)4 91 41 89 16; Tel: +33 (0)6 60 36 28 19; E-mail: barth@cinam.univ-mrs.fr

† Electronic Supplementary Information (ESI) available: [details of any supplementary information available should be included here]. See DOI: 10.1039/b000000x/

tion is, if electrons can also be explicitly transferred into supported, bulk-like C_{60} islands without any intrinsic charge transfer between the islands and the surface or dopants (adsorbed or intercalated atomic species). In other words, can we charge C_{60} islands in a direct manner with electrons, for instance with the help of an AFM tip? Such type of direct charging would open the perspective to study charge attachment, stability but also charge transport in C_{60} bulk system, which is of particular importance for applications in, e.g., photo-voltaic.

In this paper, we show that electrons can be indeed transferred on demand from the AFM tip into single bulk-like C_{60} islands. We exemplify this by controlled charge-manipulation experiments conducted by noncontact AFM (nc-AFM), electrostatic force microscopy (EFM) and Kelvin probe force microscopy (KPFM) in ultrahigh vacuum. Elementary surface charges could have been detected in the past by EFM[35,36] and KPFM[37,38] with nanometer resolution, and elementary charges have also been explicitly injected from the tip to the surface[39,40]. We conducted experiments on the (001) surface of a thick insulating bulk NaCl crystal because NaCl(001) has a large band gap of 8.5 eV[41] so that *a priori* no immediate intrinsic charge transfer can be expected between C_{60} islands and NaCl(001). We describe the charging of single C_{60} islands, the characteristics of charged C_{60} islands and time dependent charge dissipation processes, which appear within half a day due to an interaction between charged C_{60} islands and the NaCl(001) support.

2 Experimental Section

The preparation of the NaCl(001) surface, the deposition of the C_{60} molecules and the AFM experiments are conducted in one UHV chamber. Technical details of the sample preparation, nc-AFM and the two electrostatic imaging modes can be found in the Supplementary Information. In the following we summarize most important aspects of the experimental methods.

Frequency modulated noncontact AFM (nc-AFM) experiments are conducted with a room temperature AFM/STM system in a UHV chamber maintaining a base pressure in the low 10^{-10} mbar range. Conducting silicon cantilevers with a resonance frequency of 280 kHz are used, with an oscillation amplitude stabilized at some nanometers.

We use frequency modulated Kelvin probe force microscopy (FM-KPFM)[37,42] and electrostatic force microscopy (FM-EFM)[35,36] where a DC (U_{dc}) and AC voltage ($U_{ac} = 1.5$ V) with frequency $f_{ac} = 475$ Hz are applied at the sample during the nc-AFM topography imaging mode (tip is grounded). In KPFM, the DC bias voltage is varied by a Kelvin feedback loop such that the electrostatic tip-surface interaction is minimized at each point on the surface. The minimizing Kelvin voltage equals then the apparent contact potential difference U between the metallic sample holder and the tip in the presence of the NaCl insulator[43]. Thanks to the modulation technique, a second, so-called *Kelvin image* representing the Kelvin voltage at each pixel is obtained in the standard topography imaging mode. In our set-up, a bright contrast in our Kelvin images corresponds to more positive Kelvin voltages and *vice-versa*. When we image the surface in the EFM mode, we de-activate the Kelvin regulator, apply a constant DC voltage (U_{dc}), extract the amplitude of the detuning signal ($\triangle f$) at the frequency f_{ac} and record this amplitude in a separate image[35,36]. The distribution of surface charges is represented by EFM[35,36] and KPFM[37,38] images.

Millimeter thick NaCl single crystals of highest purity (size: $4 \times 4 \times 10$ mm^2) are outgased by annealing at ~ 200°C in an oven, which is located inside the UHV chamber[44]. After cooling of the crystals and the sample holder, a clean (001) surface is obtained by *in-situ* cleavage of the crystal along the (001) plane at room temperature. The crystals are then annealed again in UHV at around ~ 200°C for a few hours to put the crystal into its equilibrium charge state, as described in Ref.[38]. The C_{60} molecules are evaporated at 330°C from a Knudsen cell onto the substrate kept at room temperature, with a deposition rate of 0.3 ML/min.

3 Results

After the preparation of a clean NaCl(001) surface by UHV cleavage and following annealing of the NaCl crystal in UHV, a few hundreds of nanometer wide, atomically flat terraces and one ML high steps with a typical density of 10^8 to 10^9 steps/cm^2 are obtained on NaCl(001). Depositing 0.5 ML C_{60} onto such a surface leads to typical characteristics of C_{60} islands [Fig. 1], which have been previously described[13]: due to the weak substrate-molecule interaction and the high mobility of the molecules, the islands grow at the NaCl steps in a Volmer–Weber growth mode, leading to three-dimensional C_{60} islands with (111) top facets [Fig. 1(a)]. The islands have a lateral extension of up to 150 nm and are always completed by two molecular layers, with following uncompleted layers on the third and fourth molecular height level [Fig. 1(b) and (c)].

To analyze the charge state of such islands, we always conducted KPFM measurements because respective Kelvin images represent the distribution of surface charges[37,38]. We consider the NaCl(001) terraces as to be defect-free and charge-neutral (see Section 4) so that they always serve as a reference for KPFM measurements, expressed by the Kelvin voltage U_{NaCl}.

In general, we do not observe a preferred Kelvin contrast between the C_{60} islands and the stoichiometric NaCl(001) terraces ($\triangle U_{C60\text{-}NaCl} = U_{C60} - U_{NaCl}$), which might be due to the typically relative high noise of some hundreds of mV in the Kelvin voltage where possible small contrast differences are hidden. However, during the imaging we occasionally observe changes of the Kelvin contrastas shown in Fig. 1(d): in the scanning lines marked by the four arrows the mean Kelvin contrast changes to a bright con-

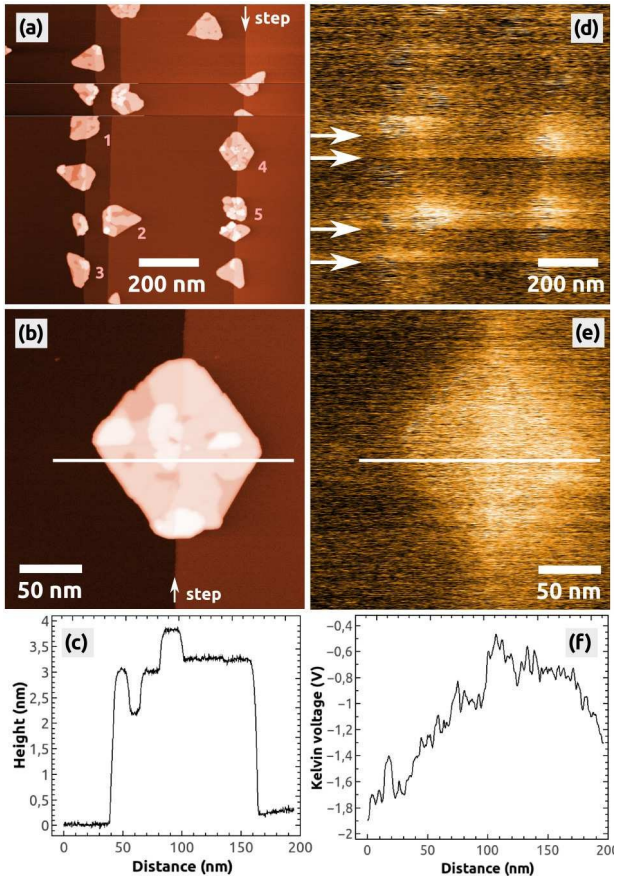

Fig. 1 Topography nc-AFM (a, b) and Kelvin images (d, e) of C_{60} islands grown at one ML high steps on the NaCl(001) surface. Images (a, d) and (b, e) were obtained each within one KPFM measurement. The height profile (c) taken from the topography image (b) exemplifies that an island can be build by up to 4 ML. The Kelvin image (d) shows that during the imaging the islands can get charged by the AFM tip, which is visible by the contrast changes (bright) marked by the arrows. The Kelvin image (e) shows that upon charging a C_{60} island a uniform bright contrast with respect to NaCl(001) is observed. Image sizes: $1 \times 1\,\mu$ m^2 (a, d), 240×240 nm^2 (b, e), speed: 0.5 Hz, $\triangle f = -21.8$ Hz.

trast , producing three bright bands. Such changes of the mean Kelvin voltage were observed and characterized before[45] and can be unambiguously assigned to changes of the electrostatic configuration of the tip apex. Because of the brighter Kelvin contrast, which corresponds to a more positive mean Kelvin voltage, we can conclude that the tip apex obviously got more positive[45]. Interestingly, such changes of the electrostatic tip configuration were not neccessarily accompanied by tip-changes visible in the topography image [compare Fig. 1(d) with (a)]. Furthermore, the tip was stable only within a few scanning lines (bright bands) but switched back after a relatively short time to its initial electrostatic configuration (dark bands).

A very important second observation is that within the bright bands a bright Kelvin contrast between the five C_{60} islands (1 to 5) and the stoichiometric NaCl(001) terraces can be observed [Fig. 1 (d)]. In following measurements, only the islands 1 to 5 appeared with a homogeneous bright contrast, as exemplified for one island by the image in Fig. 1(e): a typical homogeneously distributed bright contrast can be found, corresponding to a Kelvin voltage difference of $\triangle U_{\text{C60-NaCl}} \approx +1$ V with respect to NaCl(001) [Fig. 1(f)].

As discussed further below, the contrast phenomena visible in the Kelvin image of Fig. 1(d) can be assigned to a charging of the C_{60} islands by the tip. With respect to the Kelvin contrast formation of surface charges that have been discussed before[38], the islands obviously contained negative charges because a more positive Kelvin voltage was applied at the islands (bright contrast) with respect to the neutral NaCl(001) terraces (dark contrast).

To study charges in C_{60} islands in more detail we conducted controlled charge manipulation experiments, which are documented in Fig. 2. They were done on the same sample surface after the measurements shown in Fig. 1. We decided to charge the islands during the imaging in the EFM mode and by increasing the sample bias voltage to positive values such that negative charge from the tip is attracted towards the C_{60} islands. The topography image from a KPFM measurement in Fig. 2(a) shows two selected C_{60} islands, which are composed of 3 to 4 molecular layers [see profile in Fig. 2(b)]. The image in Fig. 2(c) of the same islands was obtained in the EFM mode at a bias voltage of $U_{\text{Bias}} = +2.0$ V, which was far beyond the Kelvin voltage of about -1 V needed to minimize the electrostatic tip-surface interaction above NaCl(001) and the islands. This means that the image in Fig. 2(c) and following EFM images [Fig. 2(e), (g) and (h)] were acquired with a relatively strong electrostatic field between the tip and the island. This explains the dark contrast of the islands with respect to NaCl(001), which probably is a result of the much smaller polarization of NaCl ($\alpha \approx 0.16$Å^3 (Na^+) and 3.1Å^3 (Cl^-)[46,47]) with respect to C_{60} ($\alpha \approx 76$Å^3[48]) in the presence of the strong electrostatic field.

The following EFM measurement [Fig. 2(e)] was obtained by scanning the surface from the bottom to the top. We first imaged the bottom island with a bias voltage of $U_{\text{Bias}} = +2.0$ V and increased slowly the voltage by a few hundreds of mV in the region marked by the arrows 1 and 2. When regulating the tip-surface distance on a constant detuning value given by $\triangle f = \triangle f_{\text{van der Waals}} + \triangle f_{\text{el}} = \text{const.}$ (constant $\triangle f$ mode), an increase of the bias voltage leads to an increase of the electrostatic contribution ($\triangle f_{\text{el}}$) and at the same time a decrease of the van der Waals contribution ($\triangle f_{\text{van der Waals}}$), which is responsible for the topography contrast. The result is that the tip is retracted from the surface leading to a fluffy topography contrast as it can be seen in the region marked by the two arrows in Fig. 2(f).

Therefore, in the scanning line at arrow 2 [Fig. 2(e)], we de-

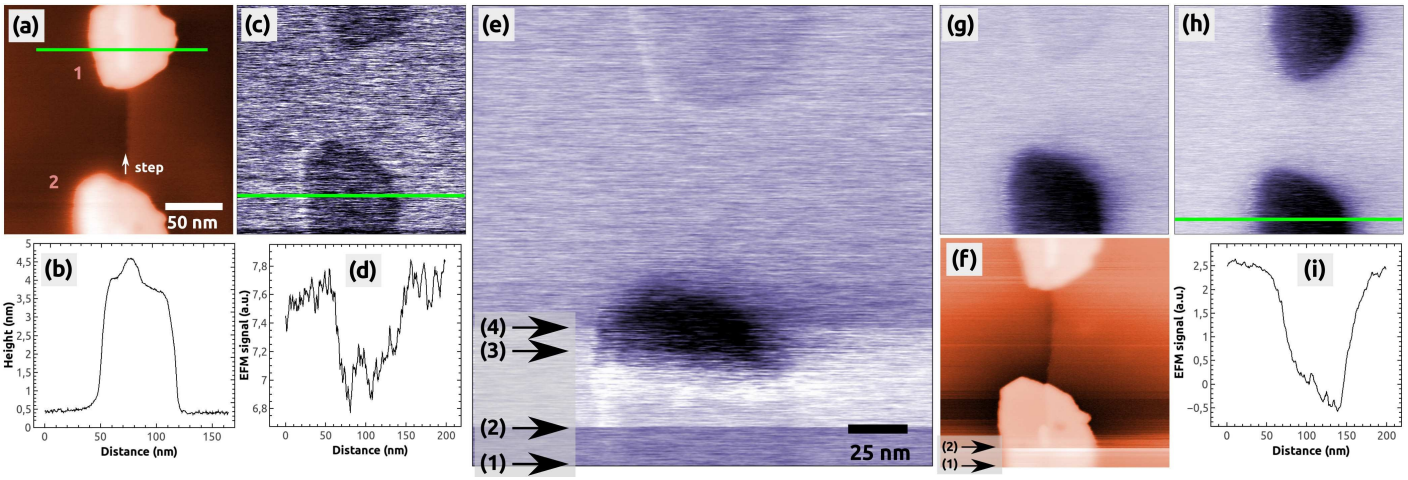

Fig. 2 The controlled charging of two C_{60} islands by the AFM tip. Both islands are located at a one ML high step of NaCl. a) Topography image of the two islands (1 and 2), with corresponding height profile (b). c) EFM image of the uncharged islands, which both exhibit a faint dark EFM contrast as shown in the profile (d). e) EFM image obtained during the charging of island 1 with corresponding topography image (f). g) EFM image after the charging of island 1. h) EFM image of the two islands after a second controlled charging of the island 2. The profile (i) shows the strong EFM contrast of island 2. Image sizes: 200×200 nm^2, speed: 0.5 Hz, $\triangle f = -7.4$ (a), -11.8 (c), -14.0 (mean value) (e, f), -13.8 (g) and -15.8 Hz (h), EFM bias voltage: $+2.0$ V (c), (g) and (h), for image (e) see text.

creased the pre-set value of $\triangle f - 14$ Hz onto the more negative value of -16 Hz (tip approach) to get back the initial sharp topography contrast of the island. In the region marked by arrows 2 and 3, the bias voltage was further increased until we reached a value of $U_{\mathrm{Bias}} = +2.5$ V (arrow 3), at which within a few scanning lines a sudden strong contrast change appeared at the island (arrow 3): the island changed its faint dark contrast to a very dark one. Immediately after this change the bias voltage was monotonously decreased within a few scanning lines onto its initially value of $U_{\mathrm{Bias}} = +2.0$ V, and at the same time, the pre-set value of $\triangle f$ was accordingly increased from -16 Hz to -12 Hz (tip retraction). No further changes of the bias voltage and detuning were done afterwards. In the last part of the image (from arrow 4 onwards) the top island still appears in its faint initial dark contrast.

The change of contrast of the bottom island can be well seen in the following EFM image [Fig. 2(g)], which was acquired with a bias voltage of $U_{\mathrm{Bias}} = +2.0$ V and without any other changes of the scanning parameters: the bottom island appears in a dark contrast whereas the top island appears in its initial, faint dark contrast. This is a clear signature that the bottom island was charged by the tip (see also below) whereas the top island remained uncharged. Note that we did not observe any topographic change of the island - the island exhibited same geometric properties in the topography images before and after the charging (see Supplementary Information, Figure S1). Note furthermore that the damping image shows a preferred contrast at the bottom island, which is discussed in the Supplementary Information (Figure S1 and S2).

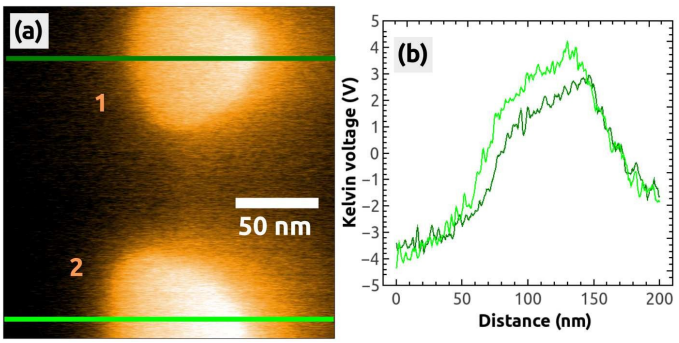

Fig. 3 A Kelvin image (a) simultaneously obtained during the acquisition of image Fig. 2(a), 2 hours after the charging of the second island 1. The profiles were taken at the green lines in image (a). Image size: 200×200 nm^2, speed: 0.5 Hz, $\triangle f = -7.4$ Hz.

In a second charging experiment, we could charge the top island with the AFM tip by following the same charging protocol described above, i.e., by applying exactly the same bias voltage of $U_{\mathrm{Bias}} = +2.5$ V. The image in Fig. 2(h) shows both islands in a strong dark contrast after the second charging [see profile in Fig. 2(i)]. After this EFM measurement, we switched to the KPFM imaging mode and obtained the Kelvin image shown in Fig. 3(a). A large contrast difference between the two C_{60} islands and the NaCl(001) terraces of up to $\triangle U_{\mathrm{C60\text{-}NaCl}} = +7$ V can be seen in the profile Fig. 3(b). Such values are a strong signature that negative charges were transferred from the tip into the islands (see Ref.[38] for contrast interpretation). Another clear signature for the con-

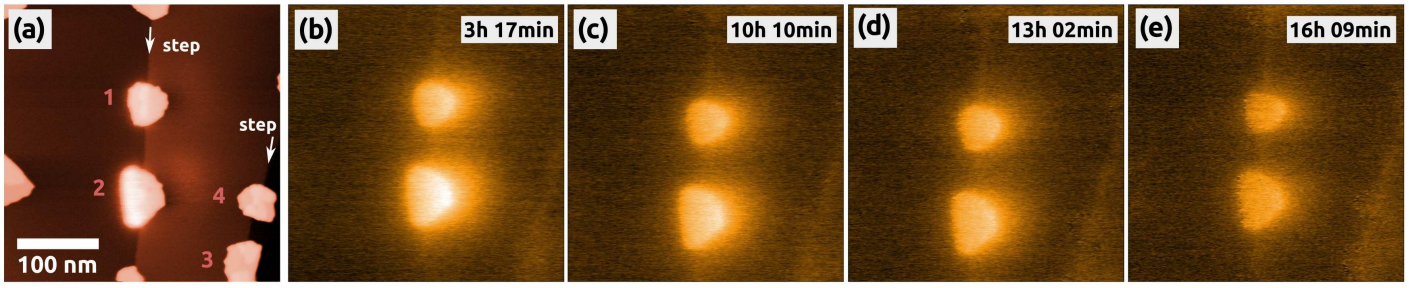

Fig. 4 The decrease of the charge inside the two C_{60} islands (1 and 2), which have been charged before by the AFM tip [see Fig. 2]. All islands are located at one ML high steps of NaCl. a) Topography and simultaneously obtained Kelvin image (b) showing also other C_{60} islands in the vicinity of the two charged islands, e.g., at 3 and 4. c)-e) Selected Kelvin images, which were obtained consecutively without changing any scanning parameters. The corresponding topography images of the latter Kelvin images are not shown. All Kelvin images have the same color scale, which ranges from -1.2 V (dark, NaCl) to $+8.0$ V (bright). The time is the one passed by after the charging of the second island (1). Image sizes: 500×500 nm^2, speed: 0.5 Hz, $\triangle f = -6.8$ Hz.

trolled charge transfer can be found in the images of Fig. 4(a) and (b), which show the same region of the surface on a larger scale (zoom out) with the charged islands located in the middle of the image at position 1 and 2, and other C_{60} islands in the vicinity (e.g., at 3 and 4): the islands in the vicinity do not exhibit any Kelvin contrast with respect to NaCl(001), which means that they were not charged during the two charging experiments. Note that the two charged islands, 1 and 2, appear in a bright Kelvin contrast gradually increasing from the left to the right, which is discussed in the Supplementary Information.

To our surprise, we could make an interesting observation: about 3h after the second charging of the top island (1) we recorded 25 measurements of the two islands within 13 hours, during which we did not change any parameters of the scanning. Fig. 4(a) and (b) is the second measurement of the series, and following selected Kelvin images from the series are shown in Fig. 4(c) to (e). All Kelvin images have the same color scale, with the reference contrast of the NaCl(001) terraces represented in one and the same color. As it can be seen, the brightness of the two charged islands decreased by time, which means that the Kelvin voltage difference between the charged islands and the NaCl(001) terraces, $\triangle U_{\text{C60-NaCl}} = U_{\text{C60}} - U_{\text{NaCl}}$, decreased from image to image. We clearly exclude a possible discharge induced by the tip because we did not observe in any of the images the typical signatures discussed for the occasional charging of islands during the scanning [Fig. 1(d)], which we expect to appear also during a discharging.

The voltage difference $\triangle U_{\text{C60-NaCl}}$ for the two islands, (1) and (2), is shown as a function of time in Fig. 5a. Starting from a high value of $\triangle U_{\text{C60-NaCl}} \approx +6.5$ V the voltage difference decreased faster for island 2 than for island 1 (from $\triangle U_{\text{C60-NaCl}} \approx +5.4$ V), whereas after about 13 hours both decreased onto a similar level of $\triangle U_{\text{C60-NaCl}} \approx +3.5$ V. Some fluctuations can be seen, which are, however, within the error bar of the values, which we extracted

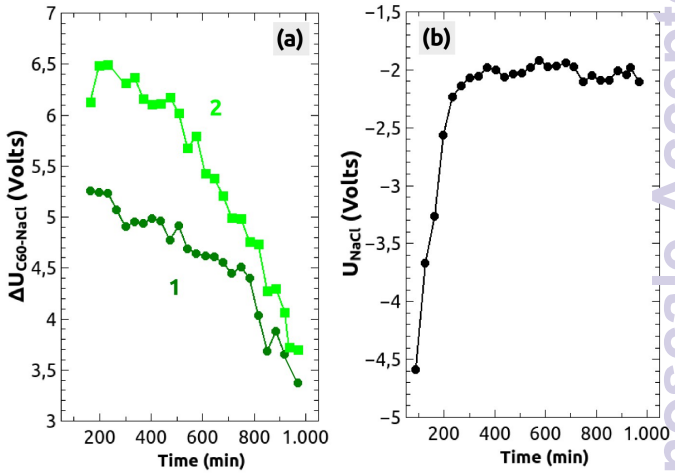

Fig. 5 a) The time dependent decrease of the charge inside the two C_{60} islands (island 1: dark green, island 2: green). b) Time dependent charge phenomena that appeared probably in the tip. In the left graph (a) the difference of the Kelvin voltages between the charged C_{60} islands and NaCl, $\triangle U_{\text{C60-NaCl}} = U_{\text{C60}} - U_{\text{NaCl}}$, is shown whereas the right graph (b) shows the Kelvin voltage between the tip and sample above the NaCl(001) surface (U_{NaCl}).

from the Kelvin images. No decrease in a staircase shape can be seen, which would otherwise point to a charge removal of single electrons as observed on Si_3Ni_4 thin films[49].

On the same time scale, the Kelvin reference voltage recorded above the NaCl(001) terrace (U_{NaCl}) shows an interesting course [Fig. 5(b)]: the voltage was first at $U_{NaCl} \approx -4.6$ V but increased after 3 hours onto a rather constant value of around $U_{NaCl} \approx -2$ V. As stated above, we consider the NaCl(001) terraces as to be charge-neutral, on which no charge phenomena take place. Therefore, the increase can only be due to a slow movement of charged defects like vacancies or dislocations below the surface[50] or more likely due to slow changes of the electronic tip configuration.

4 Discussion

4.1 Charging mechanism and condition

The experiments documented in Fig. 2 show that in general, C_{60} islands can be explicitly charged with electrons on demand by the AFM tip. From the bright Kelvin contrast at the two islands in Fig. 3 and Fig. 4 it can be concluded that electrons were transferred from the tip to the islands, which is certainly highly facilitated by the high electron affinity of bulk C_{60}. The electronic structure of bulk C_{60}, if neutral, has a semi-conducting nature[26] with the H_u band being completely filled with electrons and an empty T_{1u} band. We believe that transferred electrons are then located in the latter conduction band. Obviously, the electrons are equally distributed over the entire islands and not localized at some local positions at the islands.

The direction of the charge transfer is in agreement with the applied positive voltage of $+2.5$ V, which was more positive with respect to the minimizing Kelvin voltage of ~ -1 V: electrons in the tip are attracted towards the positive sample holder, which carries the NaCl crystal and at which the bias voltage was applied to. With respect to the tip-surface distance, we observed a relatively sharp topography contrast of the islands, which indicates that the tip had a distance of below 2 nm to the islands. Therefore, we strongly anticipate that a tunneling of electrons from the tip towards the islands appeared because of the above mentioned potential difference between the tip and the C_{60} islands and the small tip-C_{60} distance, which both increase the tunneling probability as discussed before[40,51].

We clearly stress that the charging voltage of $+2.5$ V found here may vary from experiment to experiment and in particular in dependence on the tip. We discuss this with help of the energy diagram shown in Fig. 6, in which we consider an idealized surface and tip for simplicity reasons: the NaCl(001) surface but also the representative semi-conducting Si and insulating SiO_2 tip have no defect states in their respective band gaps. The conduction and valence band of the C_{60} islands are located in the middle of the band gap of NaCl(001) due to the very large band gap of

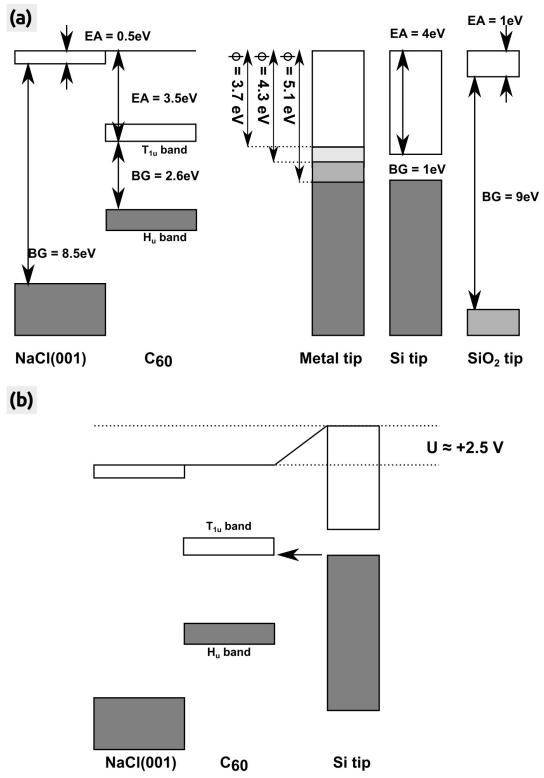

Fig. 6 Energy levels of the NaCl(001) surface, bulk C_{60} island and the AFM tip. a) All energies after a vacuum alignment. Three different tips (metal, semi-conducting Si and insulating SiO_2) are shown whereas the metal tip is represented by three different WFs ($\phi = 3.7$, 4.3 and 5.1 eV) symbolizing the WF of polycristalline magnesium, silver and gold[52]. Values for the EA and band gap (BG) were taken from literature (NaCl(001)[41], bulk C_{60}: BG[26] and EA[27,28]). For the H_u and T_{1u} bands we have taken a width of 0.9 and 0.7 eV[53]. b) Energy levels after biasing the sample with a positive voltage of $+2.5$ V. Electrons can tunnel from the conduction band of the Si tip into C_{60} (arrow). All energy levels are true to scale.

NaCl(001) and the high EA of bulk C_{60}. In this case, we can assume a vacuum alignment of the energy levels as shown in Fig. 6(a). If we now consider an active KPFM experiment, the electrostatic tip-surface interaction is minimized so that the vacuum levels of the tip and surface are aligned[43]. As shown by the three representative tips in Fig. 6(a) (metallic, Si and SiO_2 tip), no electrons can be transferred into the T_{1u} band in principle. However, when applying a more positive bias voltage (KPFM switched off) with respect to the Kelvin voltage, electrons can be transferred from the tip to the islands. This applies in particular to metal tips with a relatively low work function (WF), where a voltage below roughly $+1.5$ V is sufficient. For a Si tip, a larger bias voltage of about $+2.5$ V at the sample is needed to raise the conduction band of Si such that electrons can tunnel into C_{60} [Fig. 6(b)]. In the case of an idealized SiO_2 tip, a tunneling is almost impossible

because very large voltages are needed due to the very large band gap of 9 eV [Fig. 6(a)].

The above considerations are certainly too simplified because the composition and atomic structure of the foremost part of the tip can strongly deviate from idealized Si or SiO_2. For instance, although Si tips exposed to the ambient air carry a native oxide they are probably also hydroxilized and have defect states in the band gap which may potentially contribute to the charging. Furthermore, in typical standard room temperature experiments on NaCl(001), the tip can get contaminated by NaCl from the surface whenever the tip contacts the surface (tip changes). If a small quantity of NaCl in form of, e.g., a thin film is supported it may strongly influence, e.g., the work function of a conducting support underneath as shown for metal surfaces[54].

A very important question is how the electrons tunneled from the tip into the C_{60} islands during the controlled charging experiments in Fig. 2 and how many electrons were transferred. In principle, image Fig. 2(e) contains all information about the charging, in particular in the few scanning lines where the island 2 changed its contrast to a dark one. At these positions we could not find any signatures like an expected staircase-like transfer of single electrons from the tip to the C_{60} island[49], which was probably due to the limited time resolution of the EFM signal. An estimation of the amount of transferred electrons is therefore not possible. Electrostatic force spectroscopy as recently done[55] can help in future to observe a single electron tunneling and to count explicitly the transferred electrons. Another solution is to explicitly model the geometry composed of the NaCl(001) surface, the C_{60} island and the tip and in turn to calculate the electrostatic tip-surface interaction. However, such a calculation requires a precise knowledge of several parameters like the tip structure and composition, the tip-surface distance and the influence of the thick dielectric NaCl crystal, which are all unknown here.

4.2 Island discharge

With respect to the discharge of the C_{60} islands [Fig. 4 and Fig. 5], we can state that a discharge by the tip during imaging can be ruled out because we did not observe typical charging phenomena as documented in Fig. 1(d), which we otherwise expect to appear also during a discharging of the islands. After a charging, we never observed a topographic change of the islands - the islands always exhibited same geometric properties in the topography images (see Supplementary Information, Figure S1). This is why we exclude a possible adsorption of gas molecules from the residual gas of the UHV that could possibly reduce the charge.

The most reasonable explanation for the decrease of the island charge is based on the interaction of the charged C_{60} islands with the NaCl(001) support and more precisely, on the defect environment in the subsurface NaCl region below the islands. In principle, large defect structures such as grain boundaries or dislocations ending on the NaCl(001) surface[50] offer possible path ways for the escape of charges[56–58]. Such defects could be possibly covered by the C_{60} islands. However, we never observed grain boundaries or screw dislocations on clean (001) surfaces of our high-quality NaCl single crystals, which would have otherwise produced a clear visible contrast in topography images. For detecting $\{011\}[1\bar{1}0]$ edge dislocations[50], which have their $\sqrt{2}a_{\mathrm{NaCl}}/2$ large Burgers vector in the (001) plane, either atomic resolution can be used or even KPFM[59] since such dislocations are charged[50]. However, we never observed a Kelvin contrast on, e.g., the flat terraces which can be attributed to charged edge dislocations.

The only explanation that remains is based on the Debye-Frenkel layer[60–62], which was experimentally evidenced by KPFM[38]. A Debye-Frenkel layer is composed of positive cation vacancies (V_{Na^+}) at kink and corner sites on the surface and a space charge layer below the surface formed by divalent cation impurities like Ca^{2+}, which are contained in any NaCl crystal of even highest purity. In principle, also anion vacancies (V_{Cl^-}) contribute to the positive space charge layer because anion vacancies exist in any alkali halide even at room temperature. Both charge layers form a surface dipole, which modifies the free formation energies for cation and anion vacancies. In the presence of a charged C_{60} island this surface dipole is certainly modified such that in particular the positive anion vacancies diffuse to the negatively charged islands. The diffusion is probably also influenced by an electrostatic force gradient originating from the particular geometric shape of the C_{60} island. If so, it could be that the charge inside the islands is transferred to the positive species. In particular, anion vacancies, which are then transformed into F centers, similar to the case described for MgO[63], have a large electron affinity with a high probability to take a charge from the island[64], as it is the case for anion vacancies on MgO(001)[65,66].

5 Conclusion

In summary, we have shown that controlled charge manipulation experiments can be accomplished in UHV at single C_{60} islands with help of the AFM tip: the islands can be charged in the frequency modulated EFM mode during nc-AFM imaging by changing the bias voltage continuously to positive voltages. In our experiments we found a charging voltage of +2.5 V, which may, however, vary as a function of the electronic and structural configuration of the tip-surface system. Kelvin images show that electrons are transferred from the tip into the C_{60} islands and that the electrons are equally distributed inside the islands being responsible for the almost uniform Kelvin contrast of the C_{60} islands. The charge inside the islands decreases by time on a time scale of half a day inside the UHV, which is due to an interaction of the charged C_{60} islands with the NaCl support. A possible mechanism for this is based on anion vacancies below the sur-

face that get filled with electrons (creation of F^0 centers) at the interface NaCl-C_{60}.

Our results form a firm start in the controlled charge manipulation of bulk-like C_{60} islands on insulating surfaces, with many perspectives included. For instance, we believe that by low-temperature nc-AFM and electrostatic force spectroscopy[55] with functionalized metallic AFM tips C_{60} islands can be charged by single electron charging, which allows counting the transferred charge.

Conducting charge experiments in general helps to determine the electronic structure of charged C_{60} islands, to give answers to the maximum number of electrons that can be stored in an island (electron attachment), about stability and life-times of charges inside C_{60} and in particular to charge transport phenomena between C_{60} and its environment. We believe that charge manipulation experiments can also be done at C_{60} derivatives, which would be very interesting for applications in photo-voltaic. Our charging procedure has to be benchmarked with other self-assembled molecules to proove the generality of our concept.

Acknowledgements

We express our very great appreciation to N. Nicoara, S. Gauthier, B. Grévin and in particular to A. L. Shluger for very stimulating discussions. We highly acknowledge the French Agency for Research (*Agence Nationale pour la Recherche*) for financial support through the P3N program (project *MISS*).

References

1 H. W. Kroto, J. R. Heath, S. C. O'Brien, R. F. Curl and R. E. Smalley, *Nature*, 1985, **318**, 162–163.

2 K. M. Kadish and R. S. Ruoff, *Fullerenes: chemistry, physics, and technology*, John Wiley & Sons, Inc., 2000.

3 O. Gunnarsson, *Rev. Mod. Phys.*, 1997, **69**, 575–606.

4 S. Bosi, T. Da Ros, G. Spalluto and M. Prato, *European Journal of Medicinal Chemistry*, 2003, **38**, 913–923.

5 S. Günes, H. Neugebauer and N. S. Sariciftci, *Chem. Rev.*, 2007, **107**, 1324–1338.

6 P. A. Heiney, J. E. Fischer, A. R. McGhie, W. J. Romanow, A. M. Denenstein, J. P. McCauley Jr, A. B. Smith and D. E. Cox, *Phys. Rev. Lett.*, 1991, **66**, 2911–2914.

7 M. S. Golden, M. Knupfer, J. Fink, J. F. Armbruster, T. R. Cummins, H. A. Romberg, M. Roth, M. Sing, M. Schmidt and E. Sohmen, *J. Phys: Conden. Matter*, 1995, **7**, 8219.

8 T. Sakurai, X.-D. Wang, Q. K. Xue, Y. Hasegawa, T. Hashizume and H. Shinohara, *Prog. Surf. Sci.*, 1996, **51**, 263–408.

9 T. David, J. K. Gimzewski, D. Purdie, B. Reihl and R. R. Schlittler, *Phys. Rev. B*, 1994, **50**, 5810.

10 G. Costantini, S. Rusponi, E. Giudice, C. Boragno and U. Valbusa, *Carbon*, 1999, **37**, 727–732.

11 E. I. Altman and R. J. Colton, *Phys. Rev. B*, 1993, **48**, 18244.

12 S. A. Burke, J. M. Mativetsky, R. Hoffmann and P. Grütter, *Phys. Rev. Lett.*, 2005, **94**, 96102.

13 S. A. Burke, J. M. Mativetsky, S. Fostner and P. Grütter, *Phys. Rev. B*, 2007, **76**, 35419.

14 F. Loske, R. Bechstein, J. Schütte, F. Ostendorf, M. Reichling and A. Kühnle, *Nanotechnology*, 2009, **20**, 065606.

15 M. Körner, F. Loske, M. Einax, A. Kühnle, M. Reichling and P. Maass, *Phys. Rev. Lett.*, 2011, **107**, 016101.

16 M. Nimmrich, M. Kittelmann, P. Rahe, W. Harneit, A. J. Mayne, G. Dujardin and A. Kühnle, *Phys. Rev. B*, 2012, **85**, 035420.

17 R. Pawlak, S. Kawai, S. Fremy, T. Glatzel and E. Meyer, *J. Phys. Condens. Matter*, 2012, **24**, 084005.

18 L. Gross, F. Mohn, N. Moll, P. Liljeroth and G. Meyer, *Science*, 2009, **325**, 1110–1114.

19 C. Chiutu, A. M. Sweetman, A. J. Lakin, A. Stannard, S. Jarvis, L. Kantorovich, J. L. Dunn and P. Moriarty, *Phys. Rev. Lett.*, 2012, **108**, 268302.

20 L. Gross, F. Mohn, N. Moll, B. Schuler, A. Criado, E. Guitián, D. Peña, A. Gourdon and G. Meyer, *Science*, 2012, **337**, 1326–1329.

21 A. Rosen and B. Waestberg, *J. Amer. Chem. Soc.*, 1988, **110**, 8701–8703.

22 L.-S. Wang, J. Conceicao, C. Jin and R. E. Smalley, *Chem. Phys. Lett.*, 1991, **182**, 5–11.

23 R. Martin and J. Ritchie, *Phys. Rev. B*, 1993, **48**, 4845–4849.

24 R. L. Hettich, R. N. Compton and R. H. Ritchie, *Phys. Rev. Lett.*, 1991, **67**, 1242–1245.

25 T. Jaffke, E. Illenberger, M. Lezius, S. Matejcik, D. Smith and T. D. Märk, *Chem. Phys. Lett.*, 1994, **226**, 213–218.

26 P. Benning, D. Poirier, T. Ohno, Y. Chen, M. Jost, F. Stepniak, G. Kroll, J. Weaver, J. Fure and R. Smalley, *Phys. Rev. B*, 1992, **45**, 6899–6913.

27 M. Shiraishi, K. Shibata, R. Maruyama and M. Ata, *Phys. Rev. B*, 2003, **68**, 235414.

28 H. Ishii, N. Hayashi, E. Ito, Y. Washizu, K. Sugi, Y. Kimura, M. Niwano, Y. Ouchi and K. Seki, *Phys. Stat. Sol. (a)*, 2004, **201**, 1075–1094.

29 S. Braun, W. R. Salaneck and M. Fahlman, *Adv. Mater.*, 2009, **21**, 1450–1472.

30 S. Modesti, S. Cerasari and P. Rudolf, *Phys. Rev. Lett.*, 1993, **71**, 2469–2472.

31 R. C. Haddon, A. F. Hebard, M. J. Rosseinsky, D. W. Murphy, S. J. Duclos, K. B. Lyons, B. Miller, J. M. Rosamilia, R. M. Fleming, A. R. Kortan, S. H. Glarum, A. V. Makhija, A. J. Muller, R. H. Eick, S. M. Zahurak, R. Tycko, D. G. and F. A. Thiel, *Nature*, 1991, **350**, 320–322.

32 C. N. R. Rao, R. Seshadri, A. Govindaraj and R. Sen, *Mater. Sci. Eng.*, 1995, **R15**, 209–262.

33 A. Wachowiak, R. Yamachika, K. H. Khoo, Y. Wang, M. Grobis, D.-H. Lee, S. G. Louie and M. F. Crommie, *Science*, 2005, **310**, 468–470.

34 Y. Wang, R. Yamachika, A. Wachowiak, M. Grobis, K. H. Khoo, D.-H. Lee, S. G. Louie and M. F. Crommie, *Phys. Rev. Lett.*, 2007, **99**, 086402.

35 B. D. Terris, J. E. Stern, D. Rugar and H. J. Mamin, *Phys. Rev. Lett.*, 1989, **63**, 2669–2672.

36 R. M. Nyffenegger, R. M. Penner and R. Schierle, *Appl. Phys. Lett.*, 1997, **71**, 1878–1880.

37 C. Barth and C. R. Henry, *Nanotechnology*, 2006, **17**, S155–S161.

38 C. Barth and C. R. Henry, *Phys. Rev. Lett.*, 2007, **98**, 136804.

39 S. Morita and Y. Sugawara, *Thin Solid Films*, 2001, **393**, 310–318.

40 E. Bussmann and C. C. Williams, *Appl. Phys. Lett.*, 2006, **88**, 263108.

41 R. Poole, J. Jenkin, J. Liesegang and R. Leckey, *Phys. Rev. B*, 1975, **11**, 5179–5189.

42 S. Kitamura and M. Iwatsuki, *Appl. Phys. Lett.*, 1998, **72**, 3154–3156.

43 S. Ogawa and S. Ichikawa, *Phys. Rev. B*, 1995, **51**, 17231–17234.

44 C. Barth, C. Claeys and C. R. Henry, *Rev. Sci. Instr.*, 2005, **76**, 083907.

45 C. Barth, T. Hynninen, M. Bieletzki, C. R. Henry, A. S. Foster, F. Esch and U. Heiz, *New J. Phys.*, 2010, **12**, 093024.

46 P. Fowler and P. Madden, *Phys. Rev. B*, 1984, **29**, 1035–1042.

47 S. Pettersson and K. Subbaswamy, *Phys. Rev. B*, 1990, **42**, 5883–5886.

48 R. Antoine, P. Dugourd, D. Rayane, E. Benichou, M. Broyer, F. Chandezon and C. Guet, *J. Chem. Phys.*, 1999, **110**, 9771–9772.

49 C. Schönenberger and S. F. Alvarado, *Phys. Rev. Lett.*, 1990, **65**, 3162–3164.

50 R. W. Whitworth, *Adv. Phys.*, 1975, **24**, 203–304.

51 C. Barth and C. R. Henry, *Appl. Phys. Lett.*, 2006, **89**, 252119.

52 H. B. Michaelson, *J. Appl. Phys.*, 1977, **48**, 4729–4733.

53 E. L. Shirley and S. G. Louie, *Phys. Rev. Lett.*, 1993, **71**, 133–136.

54 S. Prada, U. Martinez and G. Pacchioni, *Phys. Rev. B*, 2008, **78**, 1–8.

55 R. Stomp, Y. Miyahara, S. Schaer, Q. Sun, H. Guo, P. Grutter, S. Studenikin, P. Poole and A. Sachrajda, *Phys. Rev. Lett.*, 2005, **94**, 056802.

56 K. P. McKenna and A. L. Shluger, *Nat. Mater.*, 2008, **7**, 859–862.

57 Z. Wang, M. Saito, K. P. McKenna, L. Gu, S. Tsukimoto, A. L. Shluger and Y. Ikuhara, *Nature*, 2011, **479**, 380–383.

58 K. P. McKenna, *J. Am. Chem. Soc.*, 2013, **135**, 18859–65.

59 P. Egberts, T. Filleter and R. Bennewitz, *Nanotechnology*, 2009, **20**, 264005.

60 K. L. Kliewer and J. S. Koehler, *Phys. Rev.*, 1965, **140**, A1226–A1240.

61 K. Kliewer, *Phys. Rev.*, 1965, **140**, A1241–A1246.

62 M. F. Butman, A. A. Smirnov, L. S. Kudin and Z. A. Munir, *Surf. Sci.*, 2000, **458**, 106–112.

63 K. McKenna, T. Trevethan and A. L. Shluger, *Phys. Rev. B*, 2010, **82**, 85427.

64 *Alexander L. Shluger, private communication*.

65 G. Pacchioni and P. Pescarmona, *Surf. Sci.*, 1998, **412**, 657–671.

66 P. V. Sushko, J. L. Gavartin and A. L. Shluger, *J. Phys. Chem. B*, 2002, **106**, 2269–2276.